Proceedings of the XII Serbian-Bulgarian Astronomical Conference (XII SBAC) Sokobanja, Serbia, September 25-29, 2020
Editors: L. Č. Popović, V. A. Srećković, M. S. Dimitrijević and A. Kovačević
Publ. Astron. Soc. "Rudjer Bošković" No 20, 2020, 69-77

TRACING THE LOCAL MORPHOLOGY OF THE MOLECULAR CLOUD ROSETTE USING MOLECULAR-LINE DATA

ORLIN STANCHEV, TODOR V. VELTCHEV and MARIYANA BOGDANOVA

Department of Astronomy, University of Sofia, James Bourchier Blvd. 5, Sofia 1164, Bulgaria
E-mail: mpetrova@phys.uni-sofia.bg, o_stanchev@phys.uni-sofia.bg, eirene@phys.uni-sofia.bg

Abstract. Recent kinematic and high-resolution observational studies of molecular clouds reveal their extremely complex, clumpy and filamentary structure. Maps of different molecular-line tracers and dust-opacity data, combined with appropriate clump-extraction methods, allow for investigation of the local morphology and its physical interpretation, e.g. to test the gravoturbulent scenario of cloud evolution. We perform a comparative analysis of two populations of clumps in the molecular cloud Rosette extracted from ^{12}CO and ^{13}CO-emission FCRAO maps. The used extraction methods differ in their concept: whether the clumps are considered as an ensemble of independent objects (GAUSSCLUMPS) or as a hierarchical set of embedded structures (DENDROGRAM). We derive basic physical characteristics of the clumps and analyze their scaling relations.

1. INTRODUCTION

Giant molecular clouds (MCs) with masses up to $10^{4\text{-}5}$ solar masses are the places where most of the stars are born in clusters shrouded by cold molecular gas and dust. They contain many smaller and denser fragments or clumps whose properties are determined by the interplay between gravity, magnetic fields and turbulent pressure. Stars form in such clumps; thus the derivation and analysis of their physical properties are important tasks for the better understanding of star formation processes.

A dominant characteristics of MCs is their hierarchical structure. Many multitracer studies have shown that the relatively small scales in that hierarchy correspond to high-density features and are invariably contained inside envelopes of lower-density gas (e.g., Blitz and Shark 1986, Lada 1992). Any given spatial scale contains more small dense structures than large sparse structures. Dense cores with size ~0.1 pc constitute the top level of the cloud hierarchy and

correspond to the scale of transition to coherent turbulence (Tafalla et al. 2004; Lada et al. 2008). Despite of the non-uniformity of the filling factor and the chemical state of MCs, the bottom of gas hierarchy can be attributed to low-density gas that fills most of the cloud volume. However, there are two main interpretations connecting the boundaries of MCs with the bottom of hierarchy. The "classical" one (Blitz et al. 2007) suggests that the cloud boundaries form clearly distinguishable bottom level of the structure hierarchy. The alternative interpretation is that the hierarchical structure continues only with chemical changes into the low-density diffuse ISM (Ballesteros-Paredes et al. 1999; Hartmann et al. 2001). Crucial factor in favor of some of these interpretations could be the lifetimes of MCs in relation to their internal crossing times, pointing to the importance of self-gravity in cloud energetics (Elmegreen 2007).

A broadly accepted approach in analysis of molecular-line data is the segmentation of the position-position-velocity (PPV) cube into physically relevant structures (population) and derivation of their characteristics. For instance, such cloud fragments/clumps are identified as connected regions of emission above a threshold intensity (Solomon et al. 1987). Some of the mostly used segmentation methods are the clump-extraction algorithms CLUMPFIND (Williams et al. 1994; water-shed segmentation technique), GAUSSCLUMPS (Stutzki & Güsten 1990; iterative fitting of three-dimensional Gaussians in the vicinity of peaks on the residuum map) and DENDROGRAM (Rosolowsky et al. 2008; application of structure trees to reveal the hierarchical connections between different size scales in MCs).

In this report we present a continuation of our analysis of clump populations in the Rosette MC derived by use of GAUSSCLUMPS from ^{12}CO/^{13}CO and *Herschel* data (Veltchev et al. 2018). Here we derive physical properties of the clump population extracted by use of the DENDROGRAM technique and compare them with those of the population of Gaussian clumps

2. OBSERVATIONAL DATA

The star-forming cloud Rosette is an appropriate object for such comparative study. Its local morphology has been intensively investigated by use of different clump-extraction methods and tracers of the molecular gas (Williams et al. 1995; Schneider et al. 1998; Dent et al. 2009; Di Francesco et al. 2010; Veltchev et al. 2018). In this work, we do not consider the expanding HII region around the young cluster NGC 2244 and the zone of its direct interaction between it and the Rosette MCs which is called 'Monoceros Ridge' (Blitz & Thaddeus 2010). Various effects of stellar feedback such as gas compression by the expanding ionization front or radiation heating from the cluster can influence physical properties of the clump population in the Monoceros Ridge region. While some studies (Schneider et al. 2012; Cambresy et al. 2013) showed that there is no indication for large-scale triggering of star-formation further inside Rosette cloud,

other reveals that more massive dense cores forms in this zone (Motte et al. 2010). The adopted distance to Rosette MC is 1.33 kpc (Lombardi, Alves & Lada 2011). We make use of ^{12}CO/^{13}CO PPV cubes taken with the 14 m telescope of Five College Radio Astronomy Observatory (FCRAO), presented and discussed by Heyer, Williams & Brunt (2006). The spectral resolutions are 0.127 km/s (^{12}CO data) and 0.133 km/s (^{13}CO data) and the angular resolution is 46 arcsec. All temperatures are given on the main beam brightness temperature scale.

3. CLUMP EXTRACTION USING DENDROGRAM METHOD

To extract the population of Dendrogram clumps, we use the PYTHON implementation of the DENDROGRAM technique called ASTRODENDRO. A dendrogram structure can be graphically represented as a tree of hierarchical objects in the data cube (Fig. 1). The tree is composed of two types of structures: *branches* or *nodes* (objects consisting of two substructures) and *leaves* (objects without substructures, associated with intensity maxima). The largest structure in the hierarchical tree is the *trunk* (or *root*).

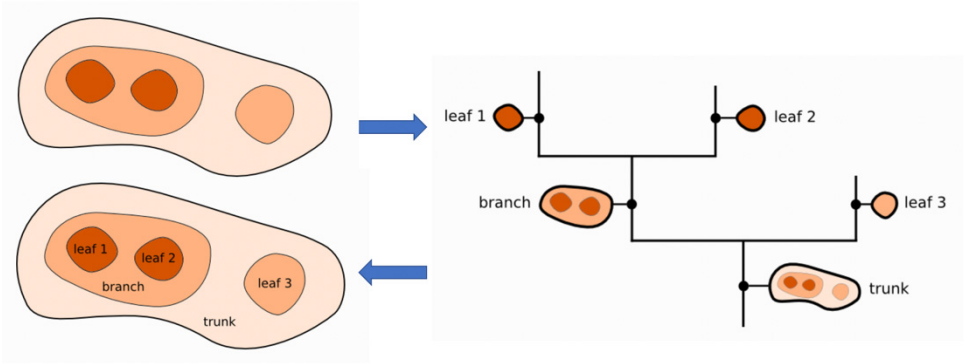

Figure 1: Illustration of a dendrogram: an arbitrary hierarchical structure (left) and the corresponding dendrogram tree (right). The trunk is the largest structure in the hierarchy and contains all other structures.

ASTRODENDRO identifies unique isosurfaces from each region in the PPV data cube and computes the properties of the delineated clump using the moment of volume weighted intensities of emission from every pixel (Rosolowsky et al. 2008). The rms sizes along the major and minor clump axis are computed from the intensity-weighted second moment in two dimensions, *dx* and *dy,* and then the effective radius is defined as the geometric mean of these second spatial moments. In a similar way, the velocity dispersion is the intensity-weighted second moment of the velocity axis. The flux of a clump is the sum of all emission within an isosurface:

$$F = \sum T_i dx dy dv,$$

where T_i is the brightness temperature. Thus, clump luminosity can be calculated as the integrated flux scaled by the square of the distance to the object:

$$L_{CO}[\mathrm{K\ km\ s^{-1}\ pc^2}] = D^2 \sum (T) dx dy dv$$

The ASTRODENDRO implementation of the DENDROGRAM technique uses three input parameters that determines the hierarchy of extracted objects: the minimum value to be considered in the data set (*min_value*), the threshold value that determines whether a leaf is a single entity or not (*min_delta*), and the minimal number of pixels for a leaf to be considered as a single entry (*min_npix*). By varying *min_value* and *min_delta,* we generated multiple clump samples to study the method's sensitivity to the choice of input parameters. As expected, large values of *min_value* produce small samples of clumps filling a reduced volume of the data cube. On the other hand, choosing too low *min_value* may lead to identification of some noise spikes in the data as physical dendrogram objects; therefore *min_value* < 2 is not recommended by the authors of the DENDROGRAM technique. The choice of *min_delta* controls how significant a leaf has to be in order to be considered as an independent entity. The measure of significance is the difference between its peak flux and the value at which it is being merged into the structure tree. Thus, the choice of *min_delta* affects the number of extracted leaves in the extracted clump sample. The default value of *min_npix* is set to six. A leaf which consists of less pixel as the dendrogram tree is being constructed is merged with a branch or another leaf and is not considered as a separate entity.

4. SPATIAL ASSOCIATION BETWEEN GAUSSIAN AND DENDROGRAM CLUMP POPULATIONS

Various tracers of cloud structure are sensitive to different ranges of density and optical depth while the specifics of a chosen clump-extraction algorithm reflect the physical processes behind the observed local cloud morphology. Therefore, spatial association (or, cross-identification) between clumps ensembles derived from different tracers and/or obtained from different clump-extraction techniques might be helpful to understand the physics of MCs. We follow the technique described in Veltchev et al. (2018) to associate Gaussian and dendrogram clump populations in the Rosette MC. Fig. 2 displays the spatial distribution of dendrogram clumps (light grey) for the choice of input parameters (*min_value* = 2 sigma, *min_delta* = 2 sigma) juxtaposed with that of Gaussian clumps (dark grey) extracted from the ^{12}CO (left) and ^{13}CO map (right). The region which includes the Monoceros ridge and the cluster NGC 2244 (shaded circle) is excluded from further analysis (see Sect. 2). As seen in Fig. 2, both Gaussian and dendrogram populations trace the `main ridge' of the Rosette MC and some of the larger filaments.

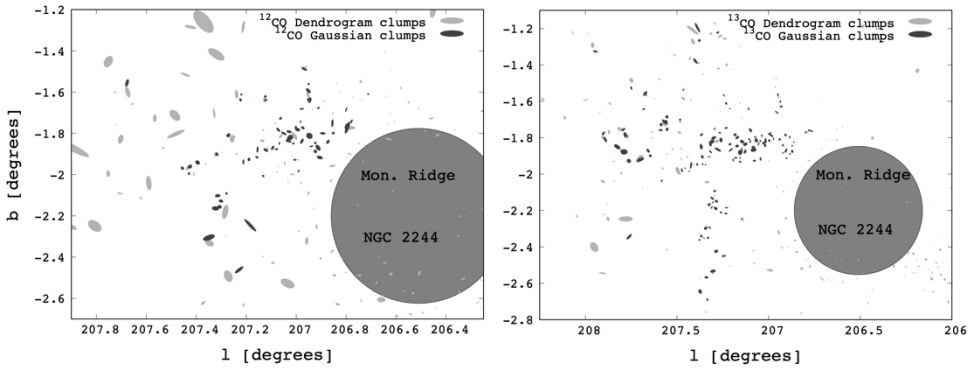

Figure 2: Spatial distributions of Gaussian (black color) and Dendrogram (grey color) clump populations for 12CO and 13CO PPV data cubes. The Monoceros Ridge zone is labeled in circle (bottom right side on the diagrams).

Let us briefly recall the technique Veltchev et al. (2018) for cross-identification between the clump populations. The overlap coefficient w between 2 clumps is defined as the intersection area, normalized to the area of the smaller ellipse (assuming elliptical geometry of the clumps). Clump pairs with $50\ \% \leq w < 90\ \%$ are defined as overlapping (type O) while those with $w \geq 90\ \%$ – as embedded (Type E). Such criteria are strong enough to ensure that most of the mass of a centrally condensed clump is contained in the overlap area. The subsequent physical analysis showed the ability of this approach to reveal essential properties of the cloud structure. We applied it for cross-identification between Gaussian and dendrogram clumps and summarize the results in Table 1.

	Total number of Gaussian clumps	Total number of Dendrogram clumps	Associated Gaussian clumps	Associated Dendrogram clumps	Number ratio (E / O)
^{12}CO	68	102	18	17	0.8
^{13}CO	130	163	51	44	1.32

In a follow-up paper we intend to provide a more detailed statistics on the cross-identification between the Gaussian and Dendrogram clump populations.

5. SCALING RELATIONS

Physical parameters of clumps in Galactic MCs and their relation to cloud structure and star formation have been investigated in numerous works. Many of these studies are dedicate on scaling relations between observable quantities like velocity dispersion and mass. In his seminal analysis, Larson (1981) derives three empirical properties of clouds and their substructures (clumps) in the Milky Way: 1) a power-law relation between velocity dispersion and size of emitting medium: $\sigma_v \propto R^{0.38}$; 2) virialization of MCs: $2\sigma_v R^2/GM \sim 1$; 3) a power-law scaling relation of the mean cloud/clump density: $n \propto R^{-1.1}$. These relations have been later put to test through observations in different molecular tracers including rotational transitions of CO and its isotopes as well tracers of dense gas like NH_3, CS, and HCN (Dame et al. 1986; Heyer et al. 2001, 2009). Many of those studies reveal power-law scaling relation of the velocity dispersion with index ranging from 0.25 to 0.75 indicating self-gravitating cloud fragments in virial equilibrium.

Fig. 3 shows the size vs. mass relations for dendrogram leaves (empty circles) from the ^{12}CO and ^{13}CO map, plotted for comparison with the Gaussian clumps (filled cirlcles) analyzed by Veltchev et al. (2018). The dendrogram samples were obtained setting the input parameters *min_value* = *min_delta* = 2σ. The sizes of the dendrogram objects were calculated adopting definition of cloud radius by Solomon et al. (1987):

$$R \approx 1.91\,\sigma_r,$$

where σ_r is the geometric mean of the second spatial moments along the major and minor axis of the clump. Then the virial mass of the dendrogram clumps is calculated as follows:

$$M_{\rm vir} = \frac{5\,FWHM_v\,R}{2\,G},$$

where the $FWHM_\upsilon$ is calculated as:

$$FWHM_v = 2\sqrt{2\,\ln 2}\,\sqrt{\sigma_v^2 + \left(\frac{\Delta v}{2\sqrt{2\ln 2}}\right)^2}$$

where the second term under the square root represents the velocity resolution term with $\Delta\upsilon$ being the velocity channel width (1.127 km/s for ^{12}CO data and 0.13 km/s for ^{13}CO data).

The masses of dendrogram objects in ^{12}CO emission seem to be systematically higher than those of the Gaussian clumps. This tendency is more pronounced for the population of leaves. A possible explanation could be the different nature of the dendrogram and Gaussian objects. While a 3D Gaussian is a more appropriate representation of high-density clumps which are better traced by the ^{13}CO emission, the dendrogram objects represent cloud fragments in their real complex shapes. The same holds even more for ^{12}CO data which are sensitive to lower

density regimes in MCs and the extracted clumps from this tracer cover more diffuse regions that possibly can contain much more mass.

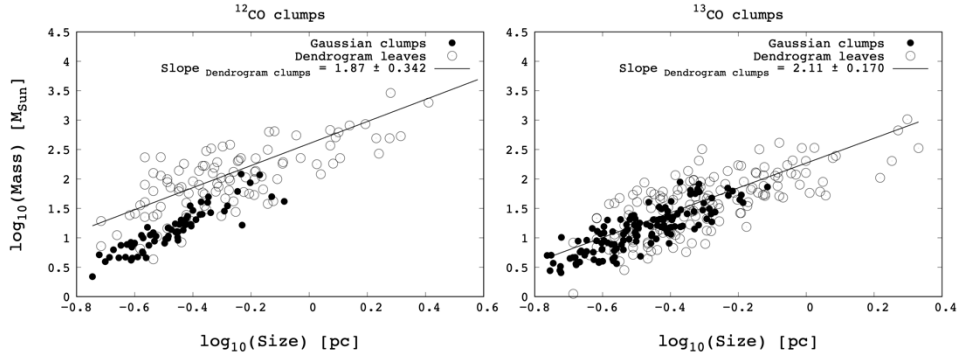

Figure 3: Size vs. mass relations for the dendrogram leaves (empty circles) and the Gaussian clumps (filled circles) from Veltchev et al. (2018). The best-fit lines for the dendrogram population are shown.

Fig. 4 displays the corresponding size vs. linewidth relations for dendrogram leaves and the associated Gaussian clumps. In general, the correlation is weak but the power index increases for the sample of dendrogram leaves associated with the Gaussian clumps from given tracer.

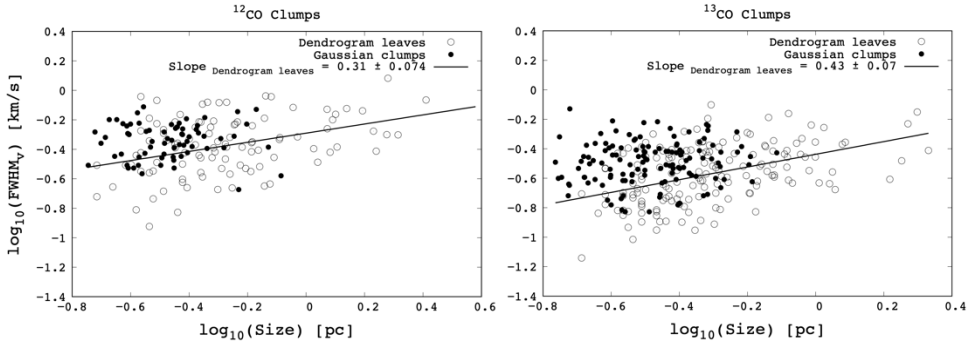

Figure 4: Size vs. linewidth relations for the dendrogram leaves (empty circles) and the Gaussian clumps (filled circles) from Veltchev et al. (2018). The best-fit lines for the dendrogram population are shown.

The summarized results for the determined slopes of the size vs. mass and size vs. linewidth relations and for three different clump populations (all dendrogram objects, dendrogram leaves only and dendrogram leaves associated with Gaussian counterparts) is shown in Figure 5.

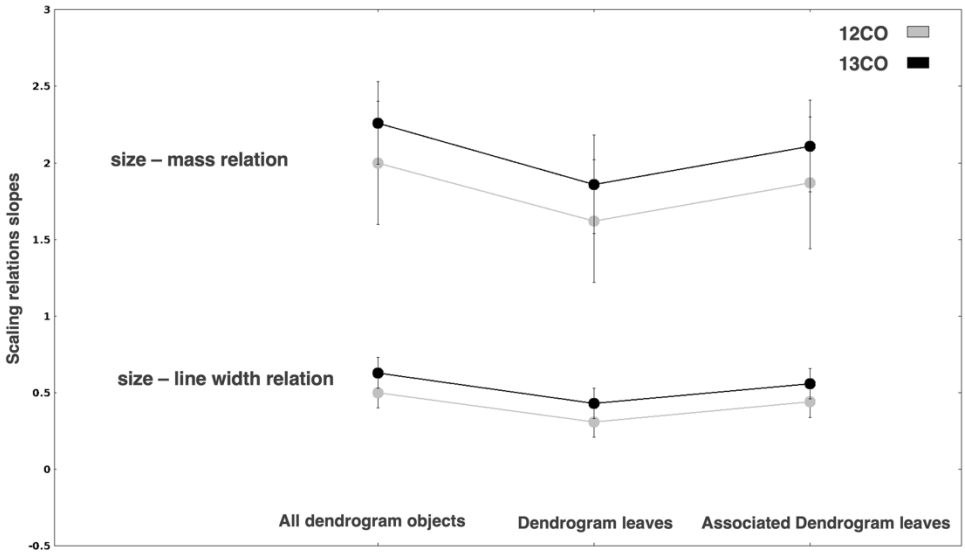

Figure 5: Summary on the derived indexes of scaling relations for clump populations extracted from the ^{12}CO and ^{13}CO maps.

6. CONCLUSION

We performed a comparative analysis of the derived properties of clump populations extracted from maps of ^{12}CO and ^{13}CO emission in the Rosette molecular cloud. Adopting the alternative extraction techniques GAUSSCLUMPS (clumps are considered as an ensemble of independent objects) and DENDROGRAM (clumps are considered as a hierarchy of embedded structures), we study the local cloud morphology, derive some basic physical characteristics of clumps and analyze their scaling relations.

The dendrogram populations exhibit shallower scaling of mass in comparison with the Gaussian clump populations whose scaling index exceeds 2.0 ± 0.3. The size vs. mass relation for the ^{12}CO populations differs from that of the ^{13}CO populations. The masses of the dendrogram objects calculated from both tracers are systematically higher than those of the Gaussian clumps; this tendency is more pronounced when one considers only the dendrogram leaves. The weak correlation of velocity dispersion with size for the dendrogram objects could be indicative of their evolutionary state.

The associated Gaussian clumps tend to have relatively high linewidths, especially considering the ^{12}CO population.

This study could be extended including the Monoceros Ridge region where the stellar feedback effects must be taken into account.

Acknowledgement

The authors are grateful to M. Heyer and J. Williams for the FCRAO molecular-line maps. This research made use of ASTRODENDRO, a Python package to compute dendrograms of Astronomical data (http://www.dendrograms.org). This research also made use of ASTROPY (http://www.astropy.org). O. Stanchev thanks to the Bulgarian National Science Fund for providing support through Grant KP-06-PM-38/6 (Fundamental research by young scientists and postdocs 2019). T. Veltchev acknowledges funding from the Ministry of Education and Science of the Republic of Bulgaria, National RI Roadmap Project DO1-277/16.12.2019.

References

Ballesteros-Paredes J., Va´zquez-Semadeni E., Scalo, J.: 1999, *ApJ*, 515, 286.
Blitz L., Fukui Y., Kawamura A., Leroy A., Mizuno N., Rosolowsky E.: 2007, in Protostars and Planets V, ed. B. Reipurth, D. Jewitt and K. Keil, Tucson, Univ. Arizona Press, 81.
Blitz L., Thaddeus P.: 1980, *ApJ*, 241, 676.
Blitz L., Stark A. A.: 1986, *ApJ*, 300, L89.
Cambresy L., Marton G., Feher O., T´oth L., Schneider N.: 2013, *A&A*, 557, 29.
Dame T. M., Elmegreen B. G., Cohen R. S., Thaddeus P.: 1986, *ApJ*, 305, 892.
Dent W. et al.: 2009, *Monthly Notices of the Royal Astronomical Society*, 395, 1805.
Di Francesco J. et al.: 2010, *Astronomy & Astrophysics*, 518, L91.
Elmegreen B. G.: 2007, *ApJ*, 668, 1064.
Hartmann L., Ballesteros-Paredes J., Bergin E. A.: 2001, *ApJ*, 562, 852.
Heyer M. H., Carpenter J. M., Snell R. L.: 2001, *ApJ*, 551, 852.
Heyer M., Krawczyk C., Duval J., Jackson J. M.: 2009, *ApJ*, 699, 1092, arXiv: 0809.1397.
Heyer M., Williams J., Brunt C.: 2006, *The Astrophysical Journal*, 643, 956.
Houlahan P., Scalo J.: 1990, *ApJS*, 72, 133.
Lada E. A.: 1992, *ApJ*, 393, L25.
Lada C. J., Muench A. A., Rathborne J. M., Alves J. F., Lombardi M.: 2008, *ApJ*, 672,.410.
Motte F., Zavagno A., Bontemps S., Schneider N., Hennemann M., Di Francesco J., Andre Ph., Saraceno P., et al.: 2010, A&A, 518, L77.
Rosolowsky E., Pineda J., Kauffmann J., Goodman A.: 2008, *The Astrophysical Journal*, 679, 1338.
Schneider N., Stutzki J., Winnewisser G., Block D.: 1998, *Astronomy & Astrophysics,* 335, 1049.
Schneider N., Csengeri T., Hennemann M., Motte F., et al.: 2012, *Astronomy & Astrophysics*, 540, L11.
Stutzki J., Güsten R.: 1990, *ApJ*, 356, 513.
Tafalla M., Myers P. C., Caselli P., Walmsley C. M.: 2004, A&A, 416, 191.
Veltchev T., Ossenkopf-Okada V., Stanchev O., Schneider N., Donkov S., Klessen R. S.: 2018, *Monthly Notices of the Royal Astronomical Society*, 475, 2215.
Williams J. P., de Geus E. J., Blitz L.: 1994, *ApJ*, 428, 693.
Williams J., Blitz L., Stark A.: 1995, *Astrophysical Journal*, 451, 252.